Effects of Central American Mountains on the Eastern Pacific Winter ITCZ and Moisture Transport*

HAIMING XU

International Pacific Research Center, University of Hawaii at Manoa, Honolulu, Hawaii, and Department of Atmospheric Sciences, Nanjing University of Information Science and Technology, Nanjing, China

SHANG-PING XIE AND YUQING WANG

International Pacific Research Center, and Department of Meteorology, University of Hawaii at Manoa, Honolulu, Hawaii

R. JUSTIN SMALL

International Pacific Research Center, University of Hawaii at Manoa, Honolulu, Hawaii

(Manuscript received 9 June 2004, in final form 5 February 2005)

ABSTRACT

The intertropical convergence zone (ITCZ) is displaced to the south edge of the eastern Pacific warm pool in boreal winter, instead of being collocated. A high-resolution regional climate model is used to investigate the mechanism for this displaced ITCZ. Under the observed sea surface temperature (SST) and lateral boundary forcing, the model reproduces the salient features of eastern Pacific climate in winter, including the southward displaced ITCZ and gap wind jets off the Central American coast. As the northeast trades impinge on the mountains of Central America, subsidence prevails off the Pacific coast, pushing the ITCZ southward. Cold SST patches induced by three gap wind jets have additional effects of keeping the ITCZ away from the coast. In an experiment in which both the Central American mountains and their effect on SST are removed, the ITCZ shifts considerably northward to cover much of the eastern Pacific warm pool.

The Central American mountains are considered important to freshwater transport from the Atlantic to the Pacific Ocean, which in turn plays a key role in global ocean thermohaline circulation. The results of this study show that this transport across Central America is not very sensitive to the fine structure of the orography because the increased flow in the mountain gaps in a detailed topography run tends to be compensated for by broader flow in a smoothed topography run. Implications for global climate modeling are discussed.

1. Introduction

The sea surface temperature (SST) exerts a strong influence on tropical deep convection: there is an empirical threshold of SST—a necessary but not sufficient condition—for atmospheric convection at 26°–27°C (e.g., Gadgil et al. 1984; Graham and Barnett 1987; Waliser and Graham 1993; Lau et al. 1997). This tight coupling between SST and convection allows strong interactions of the ocean and the atmosphere, playing an important role in shaping the tropical climate and its seasonal and interannual variations. This coupling is an important observational fact on which recent rapid progress in understanding tropical climate variability builds (see the review in C. Wang et al. 2004).

The SST–convection coupling is particularly strong over the eastern Pacific Ocean where strong gradients in SST and atmospheric sea level pressure (SLP) force low-level moisture convergence toward the SST maxi-

* International Pacific Research Center Contribution Number 314 and School of Ocean and Earth Science and Technology Contribution Number 6556.

Corresponding author address: Dr. Haiming Xu, IPRC/SOEST, University of Hawaii at Manoa, 2525 Correa Rd., Honolulu, HI 96822.
E-mail: hxu@hawaii.edu

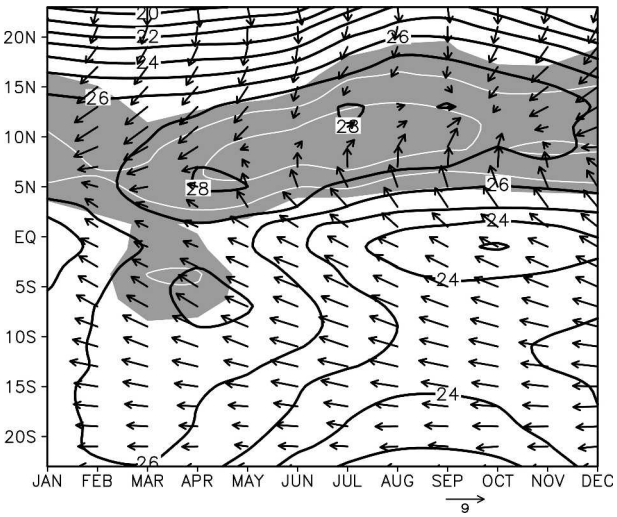

FIG. 1. Time–latitude section of climatological SST (black contours at 1°C intervals), surface wind vectors (m s^{-1}), based on COADS (Woodruff et al. 1987), averaged for 1854–1993; CPC CMAP (Xie and Arkin 1996) precipitation, averaged for 1979–2002 (white contours at 5 mm day^{-1} intervals; shade $>$ 2.5 mm day^{-1}). All zonally averaged between 120° and 115°W (from Xie 2004b).

mum. (Over the Indo–western Pacific warm pool, by contrast, the SST gradient is weak and active atmospheric convection covers only a fraction of regions where SST is above the convective threshold.) Figure 1 shows the time–latitude section of climatological SST, surface wind vectors, and precipitation, all zonally averaged between 115° and 120°W. Over the eastern Pacific, warm water with SST>26°C is confined to the north of the equator most of the time, and so is convection. Briefly in March and April, as the equatorial cold tongue relaxes (Mitchell and Wallace 1992), the meridional SST gradient weakens substantially between 10°S and 15°N, and SST south of the equator rises above the 26°C threshold, reaching as high as 27°C. Over this Southern Hemisphere warm water, considerable precipitation takes place and a double ITCZ symmetric about the equator is often observed during these months (Zhang 2001; Halpern and Hung 2001). Surface wind convergence follows the same seasonal cycle as precipitation and both are found near maximum SST. See Xie (2004b) for a recent review of coupled dynamics of eastern Pacific climate.

In the far eastern Pacific near the coast of the Americas, this SST–convection coupling displays some peculiar behavior in winter (seasons are referred to those for the Northern Hemisphere). Figure 2a presents 15-yr (1979–93) mean winter SST (Reynolds and Smith 1994) and Climate Predication Center (CPC) Merged Analysis of Precipitation (CMAP) precipitation. West of 110°W, maxima of SST and precipitation are roughly collocated, but to the east, the rainband is displaced to the southern edge of the eastern Pacific warm pool. Over a large area south of southern Mexico around 100°W, convection is suppressed despite SST exceeding 27.5°C. This ITCZ displacement south of the SST maximum in the eastern Pacific has been noted from observations by Hastenrath (1991), a result indicating that factors other than SST control the position of the ITCZ over this region. This southward displacement of the ITCZ is most pronounced in boreal winter while in summer, precipitation is generally anchored over the warmest SST (e.g., Xie et al. 2005). To our knowledge, the mechanism for this displacement has not been discussed in the literature.

Many state-of-the-art global general circulation models (GCMs), when forced by observed SSTs, fail to simulate this southward-displaced ITCZ in winter. [Rainfall distributions simulated by those GCMs that participate in the Atmospheric Model Intercomparison Project (AMIP) may be viewed online at http://www.pcmdi.llnl.gov/amip/.] In these models, atmospheric convection takes place over the eastern Pacific warm pool rather than on its south edge as observed. As a typical example, Fig. 2b shows the winter mean precipitation simulated by the National Center for Atmospheric Research (NCAR) Community Climate Model (CCM3), forced by observed global SSTs from 1979 to 1993. The simulated ITCZ compares well with observations west of 120°W, but this close coupling of SST and rainfall maxima extends too far east, all the way to the American coast.

The continents on the eastern boundary of the Pacific are highly asymmetrical with respect to the equator. The steep and high Andes separate the Pacific from much of the South American continent and the Atlantic while a mountain range runs through the narrow Central American land bridge as an extension of the Sierra Madre Occidental from North America. These Central American mountains are above 1 km high on average but only 100 km or less in width, and their orographic effect is poorly represented in global GCMs with a typical resolution of 2.8°. Three major gaps interrupt this mountain range: at the isthmus of the Gulf of Tehuantepec, over Lake Nicaragua, and at Panama (Fig. 3).

We hypothesize that the southward-displaced ITCZ might be closely related to the effects of the Central American mountain range. In winter, the northeast trade winds prevail on both sides of Central America. Blocked by the mountains, northeast winds rush through narrow mountain gaps, forming three intense

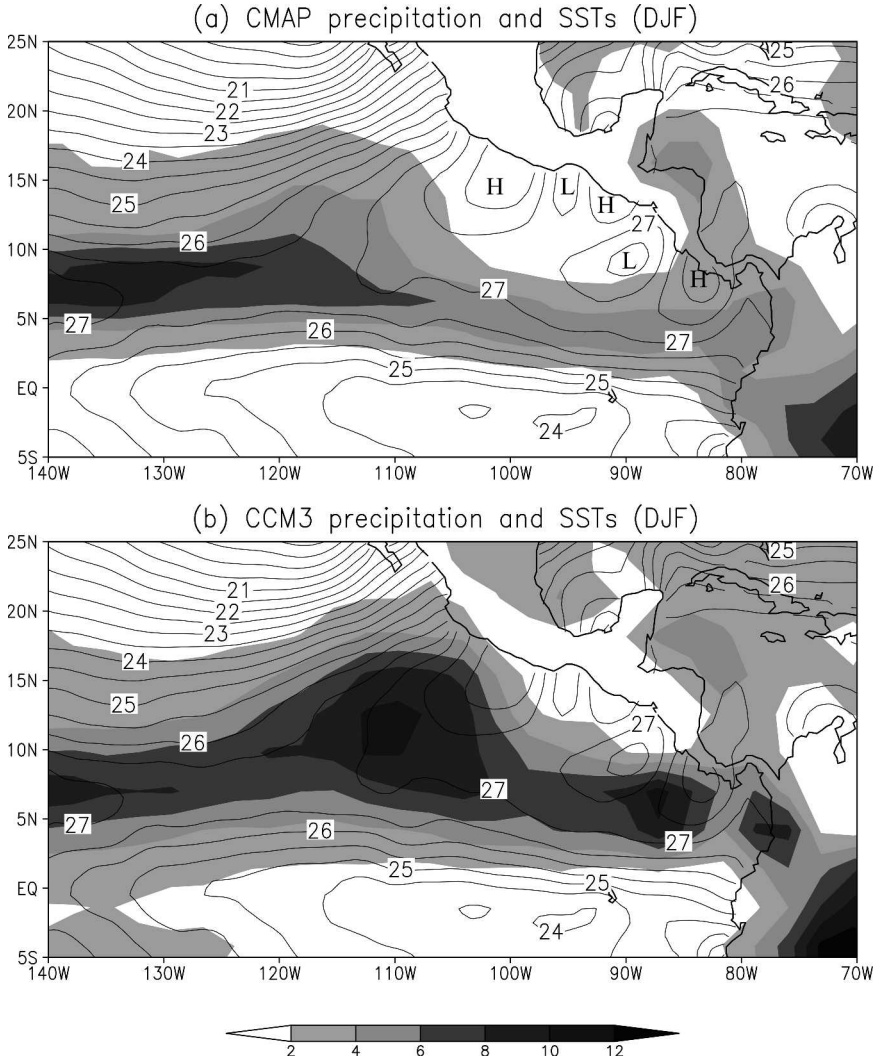

FIG. 2. Seasonal mean (DJF) precipitation (shaded, 2 mm day^{-1} intervals) for (a) CMAP observations, and (b) CCM3 simulations with global observed SSTs as surface boundary conditions, averaged for 1979–93. Seasonal mean (DJF) Reynolds SSTs are also plotted in contours at 0.5°C intervals. (The CCM3 simulated precipitation is available online at http://www.cdc.noaa.gov and based on 12 ensemble simulations.)

jets[1] offshore over the Pacific (Clarke 1988; Steenburgh et al. 1998; Chelton et al. 2000). These wind jets cause the ocean surface to cool through strong surface evaporation and entrainment of cold water from the thermocline, as reflected in three cold patches off the Gulfs of Tehuantepec, Papagayo, and Panama (Xie et al. 2005, their Figs. 4 and 6). These cold patches may keep the ITCZ from getting close to Central America. Furthermore, the trade winds probably flow over the mountain range, generating subsidence in the lee over the Pacific. The trade winds are strongest in winter, and probably so is orographic subsidence over the Pacific, a seasonality consistent with the observations that the ITCZ's displacement from the warm pool is most pronounced in winter (Xie et al. 2005).

The present study investigates the cause of the ITCZ's southward displacement from the eastern Pacific warm pool off Central America, and tests the above hypothesis of orographic subsidence and SST cooling using a full-physics regional climate model. Compared to global GCMs, the regional model can afford higher resolution to better resolve the narrow

[1] The term "jet" in this study is defined subjectively to be a localized region of strong offshore winds in the lee of the three low-elevation gaps through the Central American mountain range.

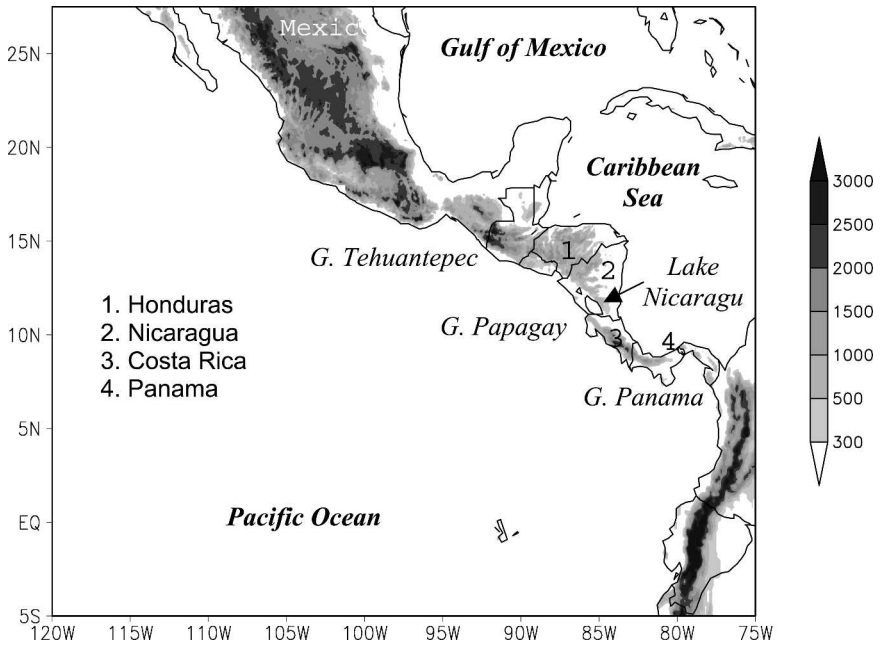

FIG. 3. Map of topography (shaded, interval levels 300, 500, 1000, 1500, 2000, 2500, 3000 m) based on the 5 min. × 5 min. U.S. Navy ETOP5 data and geographical locations referred to in this paper.

mountains—the 0.25° grid size we use is equivalent to a T480 resolution for a global spectral model. Our results show that indeed, the Central American mountains exert a significant influence on eastern Pacific warm pool convection, through both the direct orographic subsidence and indirect effect on SST.

Central America is one of the main regions where moisture is fluxed from the Atlantic to the Pacific Oceans, due to the favorable northeasterly wind direction and the relatively low mountains compared to the Andes and Rockies. This moisture transport is balanced only partly by the eastward transport in the extratropics, causing a net loss of freshwater in the Atlantic and rendering its salinity much greater than that in the Pacific. Broecker (1997) argues that this is the major reason why the North Atlantic is favored for deep-water formation that drives the global thermohaline circulation. Hence it is important for climate models to make good estimates of this Atlantic-to-Pacific flux. In this study we use the results from the regional model to investigate the sensitivity of the flux to model orography.

The rest of the paper is organized as follows. Section 2 describes the model, experimental design, and observational data sets used for verification. Section 3 presents the simulation results and investigates the effects of the Central American mountains on precipitation. Section 4 investigates the sensitivity of moisture flux estimates to model resolution and the representation of orography. Section 5 is a summary and discusses broad implications.

2. Model and experimental design

a. Model

The regional climate model (RCM) developed at the International Pacific Research Center (IPRC), University of Hawaii, is used in this study. It is a primitive equation model with sigma as the vertical coordinate, solved on a longitude–latitude grid system. The model domain is 10°S–27.5°N, 125°–65°W, including the eastern Pacific, Mexico, Central America, the Gulf of Mexico and Caribbean Sea, and part of South America (Fig. 4). The model uses a grid spacing of 0.25° in both longitude and latitude, and has 28 levels in the vertical. A detailed description of the model and its performance in simulating regional climate of East Asia can be found in Wang et al. (2003). The model has also been used to simulate the regional climate over the eastern Pacific, including the atmospheric response to tropical instability ocean waves (Small et al. 2003), boundary layer clouds over the southeast Pacific (Y. Wang et al. 2004), and the effect of the Andean mountains (Xu et al. 2004).

The model includes a detailed cloud microphysics scheme for grid-scale moist processes (Wang 2001).

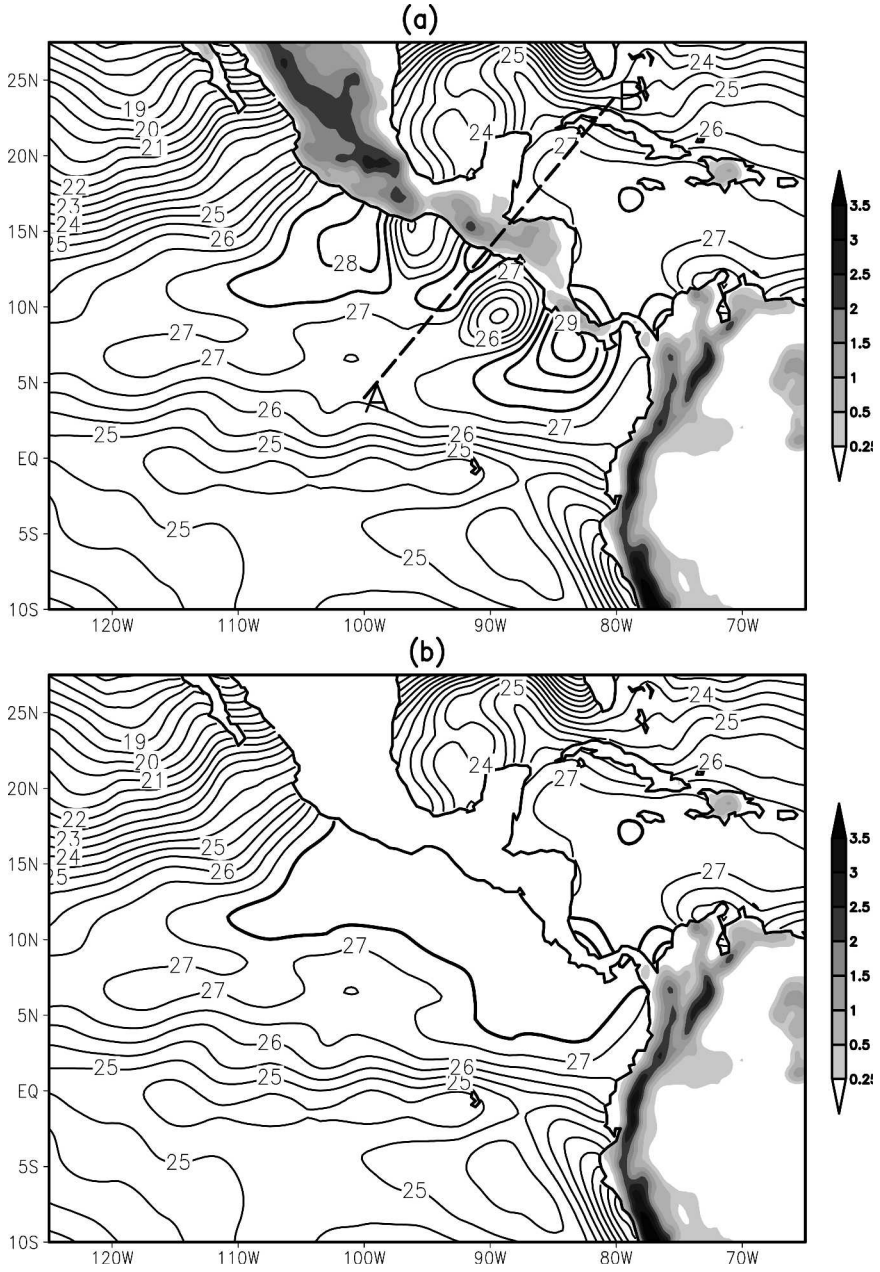

FIG. 4. Model domain and topography (shaded, interval levels 0.25, 0.5, 1.0, 1.5, 2, 2.5, 3, 3.5 km) for (a) CTL and (b) NoTop runs. 2-month (Jan and Feb 2002) mean SSTs (contours at 0.5°C intervals) for (a) CTL and (b) NoTopSmSST runs are also plotted.

The mixing ratios of cloud water, rainwater, cloud ice, snow, and graupel are all prognostic variables in the model. Condensation (evaporation) of cloud water takes place instantaneously when the air is supersaturated (subsaturated). Subgrid-scale convective processes, such as shallow convection, midlevel convection, and penetrative deep convection, are considered based on the mass flux cumulus parameterization scheme originally developed by Tiedtke (1989) and later modified by Nordeng (1995).

The subgrid-scale vertical mixing is accomplished by the so-called E–ε closure scheme, in which both the turbulence kinetic energy (TKE) and its dissipation rate are prognostic variables (Detering and Etling 1985). Turbulent fluxes at the ocean surface are calculated using the TOGA COARE algorithm (Fairall et al.

1996). Over the land, the bulk aerodynamic method is used in the land surface model, which uses the Biosphere–Atmosphere Transfer Scheme (Dickinson et al. 1993). Soil moisture is initialized using a method described by Giorgi and Bates (1989) such that the initial soil moisture depends on the vegetation and soil type defined for each grid cell.

The radiation package originally developed by Edwards and Slingo (1996) and later modified by Sun and Rikus (1999) is used, which includes seven/four bands for longwave/shortwave radiation. Seasonal-varying climatological ozone and a constant mixing ratio of carbon dioxide for the present climate are used.

b. Experimental design

The initial and lateral boundary conditions are obtained from the (National Centers for Environmental Prediction) NCEP–NCAR global reanalysis (Kalnay et al. 1996), available on a 2.5° × 2.5° grid with 17 vertical pressure levels. They are interpolated onto the model grid by cubic spline interpolation in the horizontal and linear interpolation in both the vertical and time based on four times daily reanalysis. Over the ocean, the NOAA optimal interpolation V2 weekly SST dataset on a 1° × 1° grid is used as the lower boundary condition (Reynolds et al. 2002).

The following four experiments are carried out to examine the effects of the Central American mountains on the eastern Pacific ITCZ and moisture transport. Each experiment is initialized at 0000 UTC on 1 January 2002, and integrated for 2 months. The rest of the paper discusses the January–February means constructed from hourly output (the output for the first 3 days is discarded and referred to as model spinup).

- *Control (CTL) run*. The model topography is based on the U.S. Geophysical Survey 0.0833° × 0.0833° topographic dataset and smoothed with an envelope topographic algorithm (Wang et al. 2003). At our model resolution, the main features of Central American cordillera are reasonably represented (Fig. 4a). The mountains are about 2 km high in Mexico and 1 km high in Central America, but somewhat too low represented in Costa Rica and Panama.
- *No-topography (NoTop) run*. The mountains of Central America and Mexico are removed by setting land elevation at 0.5 m (Fig. 4b). Strictly speaking, the design of this no-topography run may be physically inconsistent with the imposed lateral boundary conditions that are influenced by the presence of these Central American mountains in the first place. Nevertheless, a comparison of the CTL and NoTop runs can help identify the mountain effects within the context of this model.
- *No-topography and smoothed SST (NoTopSmSST) run*. While the comparison of the CTL and NoTop runs can identify the direct effect of the Central American mountain range, these mountains leave marked signatures in the SST field in the form of three cold patches through the action of gap wind jets (Fig. 4a). These cold patches, along with warm patches leeward of mountains, in turn affect the atmospheric circulation and convection, and may be considered as an indirect effect of Central American cordillera. In the NoTopSmSST run, we remove these orographically induced variations in SST as well as the mountains themselves. The smoothed SST field is obtained by first setting SST to 27.8°C (27.5°C) if it is greater (smaller) than this value off the west coast of Central America—up to 600 km offshore, and then applying a 5-point smoother 5 times in the coastal region. Figure 4b shows the resultant SST field that is nearly uniformly above 27.5°C near the Central American coast.
- *Smoothed-topography (SmTop) run*. This experiment is identical to the CTL run except that the topography is replaced with a smoother one taken from a GCM with triangular truncation at zonal wavenumber 42 (T42). The T42 topography is interpolated onto the model grid by cubic spline interpolation. To be consistent with the land–sea mark in the regional model, nonzero topography heights over the ocean are set to zero, because the T42 topography extends to the ocean, especially over the eastern Pacific off the west coast of Central and South Americas. This simulation is used to investigate the effect of topographic resolution on the moisture transport from the Atlantic to the Pacific.

c. Observational data

To evaluate the model simulations, we use precipitation rate and column-integrated water vapor measured by the Tropical Rainfall Measuring Mission (TRMM) Microwave Imager (TMI). TMI satellite measures SST, rain rate, and water vapor over the Tropics within 38°N–S, at resolutions of 0.25° in space and twice daily in time. We use a monthly TMI product available since January 1998 on a 0.25° grid (Wentz et al. 2000). Serra and McPhaden (2003) compare TMI precipitation with self-siphoning rain gauge data from 14 open-ocean buoys located in heavy-rain areas of the tropical Pacific and Atlantic Oceans, and report a favorable comparison on monthly and seasonal time scales. The TMI product is only available over the oceans, and in order to evaluate the modeled rainfall over land, we use

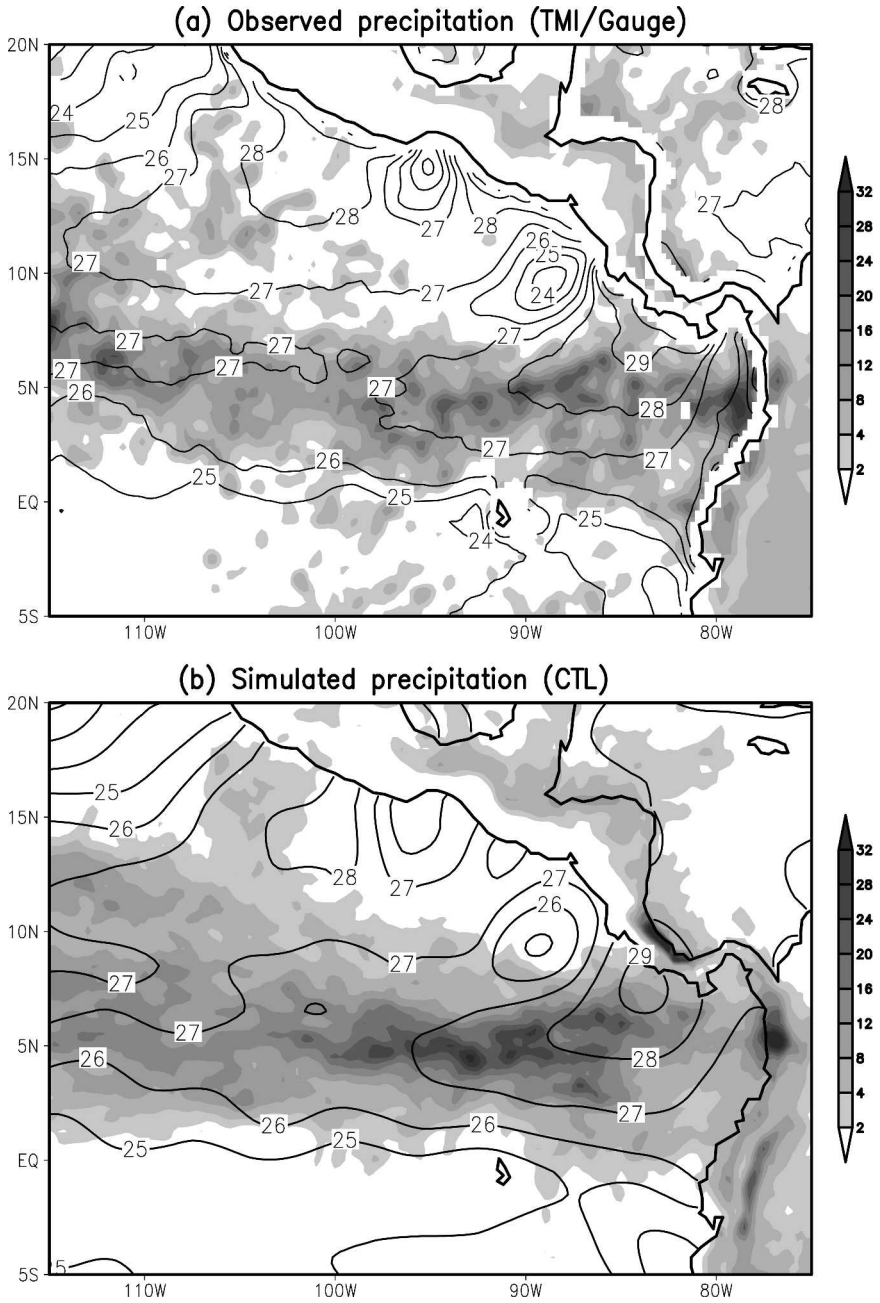

FIG. 5. The 2-month (Jan–Feb) mean daily precipitation (shaded, interval levels 2, 4, 8, 12, 16, 20, 24, 28, and 32 mm day^{-1}) for (a) TMI observations over the ocean in 2002 and gauge-corrected precipitation over the land, averaged for 1950–99, and (b) model CTL run. The 2-month (Jan–Feb 2002) mean (a) TMI and (b) Reynolds SSTs (contours at 1°C intervals) are also plotted.

a monthly terrestrial precipitation product from University of Delaware Center for Climatic Research (Legates and Willmott 1990) that is based on station records and available on a 0.5° × 0.5° of latitude/longitude grid from January 1950 to December 1999. The monthly Climate Predication Center (CPC) Merged Analysis of Precipitation (CMAP; Xie and Arkin 1996) dataset on a 2.5° grid is also used. The monthly CMAP precipitation is available since January 1979.

The microwave scatterometer on the Quick Scatterometer (QuikSCAT) satellite measures surface wind ve-

locity over the World Ocean (Liu et al. 2000). We use a monthly product for wind velocity available since August 1999 on a 0.25° grid. TMI and QuikSCAT observations have revealed rich structures on short spatial scales around the world (Xie 2004a; Chelton et al. 2004).

3. ITCZ experiment results

a. Control run

Figure 5 compares the simulated precipitation averaged for January–February 2002 with the TMI observations over the ocean for the same period. In January–February, major precipitation in the eastern Pacific occurs in the zonally elongated ITCZ centered around 5°N, a feature that the model reproduces reasonably well. The simulated ITCZ is visibly displaced to the south of maximum SST, especially between 100° and 110°W, a feature most GCMs fail to simulate. However, the simulated ITCZ is slightly stronger and wider than the observed counterpart (Fig. 5a). The simulated precipitation is also found over the Caribbean Sea on the windward side of the Central American mountain range. This orographic-induced precipitation is confirmed by January–February mean climatology[2] (Fig. 5a) of gauge measurements from 1950 to 1999 (Legates and Willmott 1990). Pierrehumbert and Wyman (1985) and Mozer and Zehnder (1996) study the effects of mesoscale mountains on flow adjustment and discuss the conditions for flow-over and flow-around regimes. Adjustment across Central America displays the characteristics of both regimes. The windward rainband in observations and the model suggests upward motion on the Caribbean side of the mountains and a flow-over component in winter. The strong wind jets through the mountains gaps, on the other hand, are indicative of flow-around.

The simulated 10-m surface wind velocity field generally compares well with the QuikSCAT observations (Fig. 6). In particular, the model captures strong wind jets off Tehuantepec and Papagayo and reduced wind speeds leeward of the mountain barrier. The Tehuantpece and Papagayo jets extend over a few hundred kilometers offshore, and eventually merge into the Pacific northeast trades. The Tehuantepec jet is oriented roughly in the north–south direction while the Papagayo jet takes a more zonal orientation. This difference in orientation between these jets greatly affects ocean dynamic response and its delayed effect on summer atmospheric convection (Xie et al. 2005). The simulated

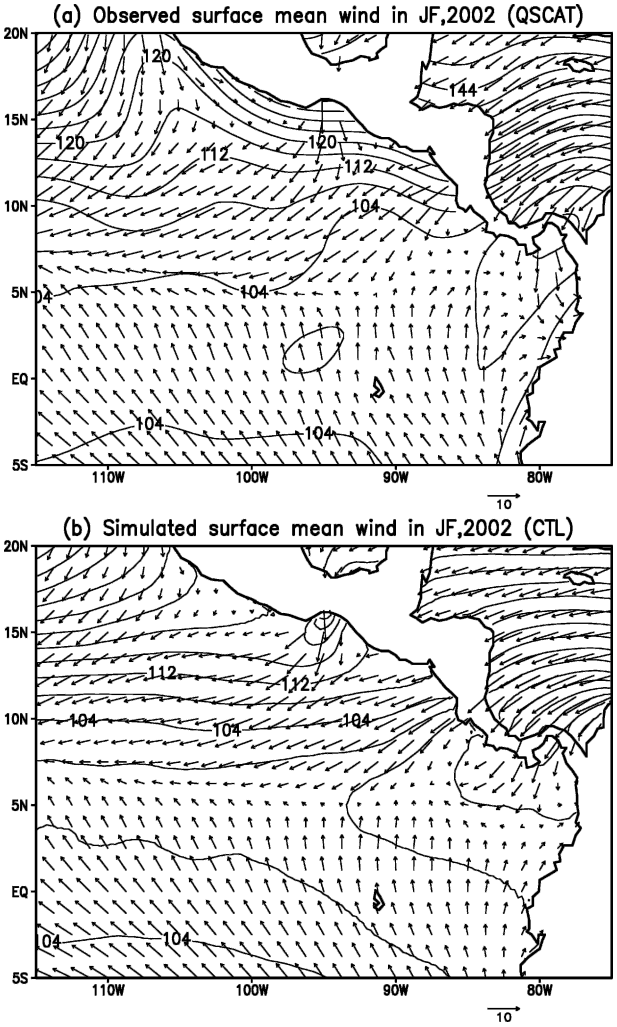

FIG. 6. The 10-m height wind vectors for (a) QuikSCAT observations and (b) model CTL run, averaged for Jan and Feb 2002. The 2-month mean (a) NCEP and (b) model geopotential heights (contours at 4 gpm intervals) at 1000 hPa are also plotted.

Panama jet, however, is too broad and takes a southwest–northeast orientation compared to a northerly jet in QuikSCAT measurements (Fig. 6a). These deficiencies are due in part to the coarse resolution of the model that does not adequately resolve the mountains in Costa Rica.

The simulated Tehuantepec wind jet appears to turn anticyclonically westward after leaving the coast. The fanlike wind pattern closely resembles that observed (Fig. 6a) rather than a narrow and confined jet as suggested by the scale analysis presented by Clarke (1988). A ridge of geopotential height is located over the Gulf of Tehuantepec with its pressure gradient nearly parallel to the coastal jet axis (Fig. 6b), indicating the northerly Tehuantepec jet is accelerated by the pressure gra-

[2] TMI precipitation product is not available over land.

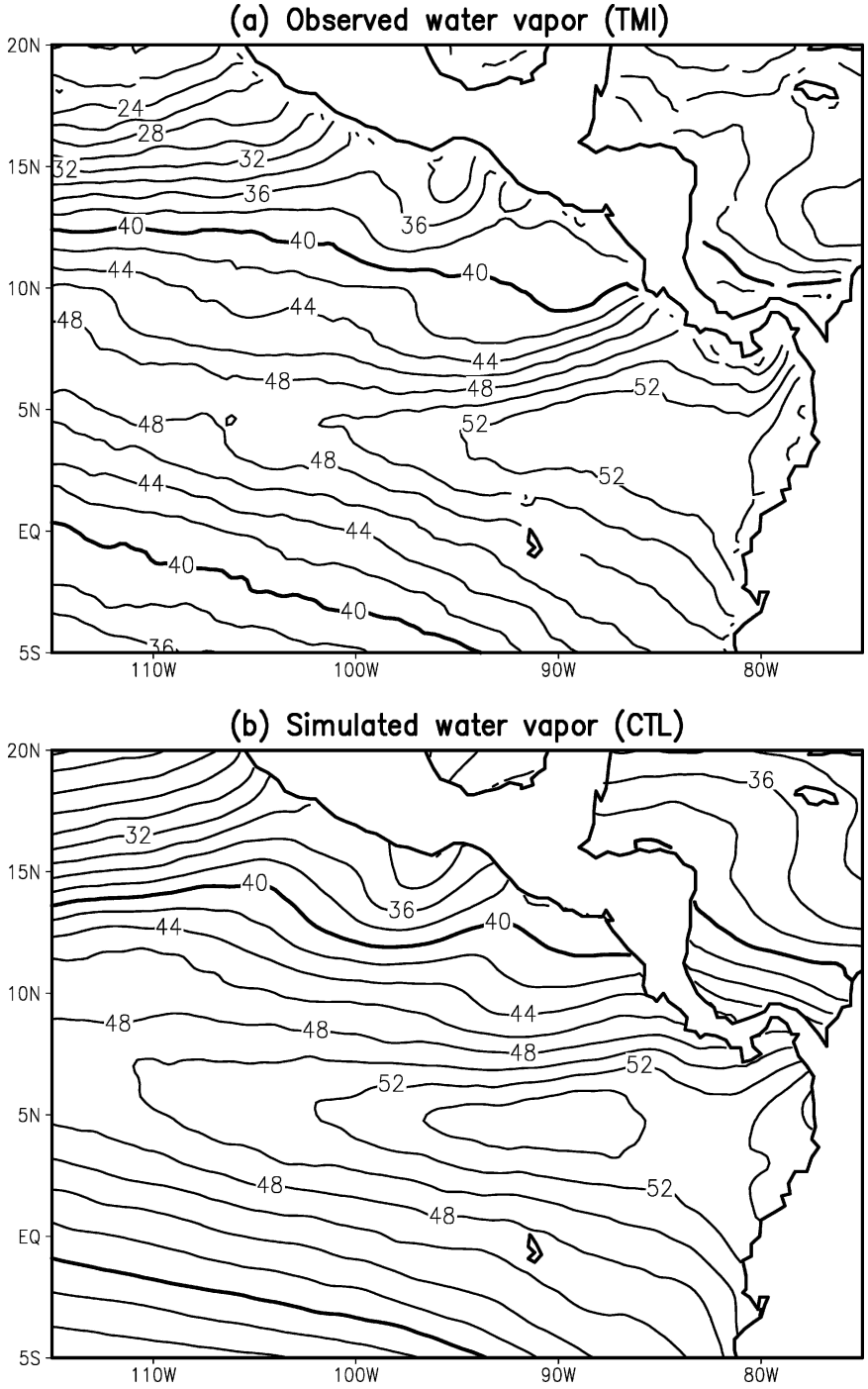

FIG. 7. Column-integrated water vapor (mm) for (a) TMI observations and (b) model CTL run, averaged for Jan and Feb 2002. Contour interval is 2 mm.

dient. Steenburgh et al. (1998) examined the momentum balances of flow curvature during a gap-outflow event over the Gulf of Tehuantepec and found that trajectories along the axis of the outflow jet were inertially balanced, but the momentum balances along trajectories off the axis of the outflow jet were modified by cross-flow pressure-gradient accelerations. Because of the influence of these cross-flow pressure-gradient accelerations on trajectories off the jet axis, the flow fans out in the outflow region rather than maintaining a

narrow jet. The simulated Tehuantepec jet finally comes into a near-geostrophic balance about 500–600 km offshore, a distance comparable to the Rossby radius of deformation. However, the geopotential height ridge does not appear along the Tehuantepec jet in the NCEP reanalysis because of its coarse resolution (Fig. 6a). Major discrepancies between the regional climate model simulation and NCEP reanalysis are also found in geopotential height west of Mexico. The trough offshore in the reanalysis is probably spurious and in violation of geostrophy with the wind velocity observed by QuikSCAT west of Mexico. There, the simulated winds are weaker than the QuikSCAT winds, especially along the coast, but their directions are roughly consistent.

The characteristics of the Papagayo jet seem to be fundamentally different from the Tehuantepec jet. The Papagayo jet does not turn to the north anticyclonically after exiting the gap and geopotential height contours are almost parallel to the direction of the Papagayo jet (Fig. 6b), indicating a near-geostrophic balance. Chelton et al. (2000) suggested that this different character of the Papagayo jet might be because the gap over the Nicaraguan lake is wide enough for the trade winds to maintain a near-geostrophic balance across Central America.

Figure 7 compares the column-integrated water vapor content between the TMI observations (Fig. 7a) and the model simulation (Fig. 7b). The model reproduces well the high water vapor content in the zonal-oriented ITCZ between 2.5° and 7.5°N, except for a slight overestimation. Over the Northeast Pacific off Central America, the simulated water vapor compares reasonably well with the TMI observations both in spatial distribution and magnitude. In particular, the dry tongue over the Gulf of Tehuantepec is well reproduced in the model as a result of dry advection from the north. Over the Pacific between 10° and 15°N, water vapor content both in the model and observations decreases near the west coast of Central America, indicating that the orographically induced rainfall on the windward side and downdraft in the lee may play an important role in reducing water vapor as the northeast trades impinge upon Central America.

b. Topographic effects

With the Central American mountain range removed in the NoTop run, the surface wind and precipitation distributions are markedly changed. Without the mountain barrier, air flows freely across Central America, and the northeast trade winds become very smooth in space over the Northeast Pacific (Fig. 8), in contrast to large variations in the CTL run. A near-geostrophic balance is maintained over both the Caribbean Sea and the eastern Pacific. Compared to the CTL run the ITCZ rainband shifts markedly northeastward and becomes broader in the meridional direction, especially over the warm water south of Mexico between 110° and 100°W (Fig. 9a). Without the direct orographic effect, the SST effect on precipitation becomes much clearer than that in the CTL run. Besides occupying the warm water south of Mexico, rainfall reaches a distinct maximum in a zonally oriented band of high SSTs between the Papagayo and Panama cold patches. The precipitation rate in this zonal rainband is significantly greater than that in the CTL run. On the other hand, precipitation remains low over the Tehuantepec and Papagayo cold patches, producing two holes in the broad ITCZ. The orographic effect on the eastern Pacific ITCZ can be seen more clearly in the (CTL minus NoTop) precipitation difference map (Fig. 10). A pair of zonally oriented bands of rainfall anomalies, positive and negative roughly south and north of 5°N, respectively, indicates that the mountains act to push the eastern Pacific ITCZ southward. On the windward side of the mountains, rainfall increases in the CTL run compared to the NoTop run because of orographic lifting.

Now we examine further the mechanism by which the Central American mountain range displaces the eastern Pacific ITCZ southward. Figure 11 shows cross sections of model results along the line AB as marked in Fig. 4a. The mountains force a strong updraft on the windward side (Fig. 11a) with elevated cloud liquid water content (Fig. 11a) and precipitation (Fig. 5). On the leeside, the mountains cause a strong downdraft, which along with the windward precipitation depresses spe-

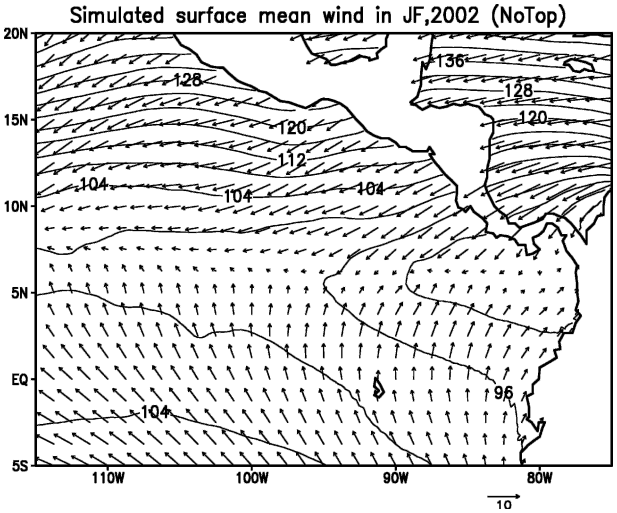

FIG. 8. The 10-m height wind vectors and geopotential heights (contours at 4 gpm intervals) at 1000 hPa for model NoTop run, averaged for Jan and Feb 2002.

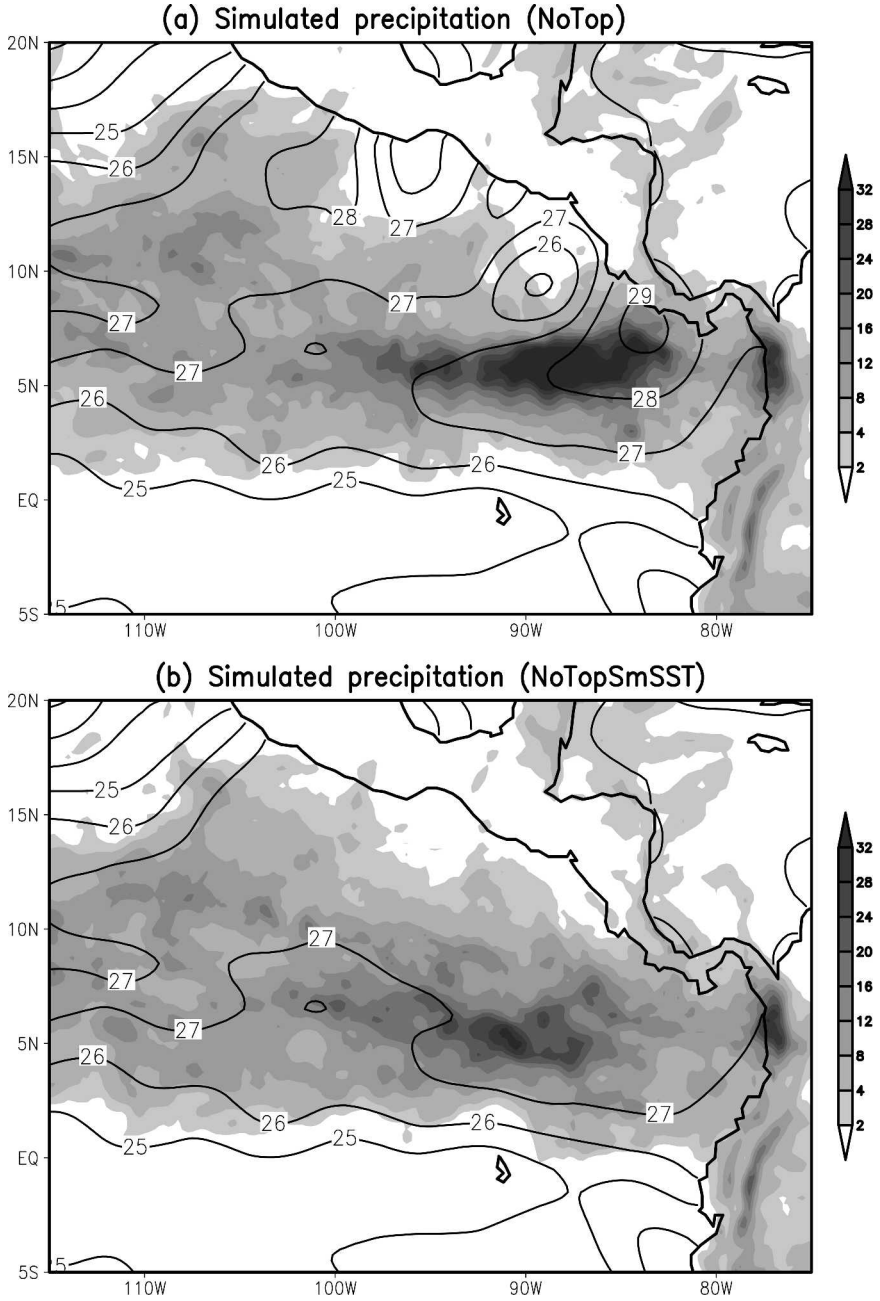

FIG. 9. The 2-month (Jan and Feb 2002) mean daily precipitation (shaded, interval levels 2, 4, 8, 12, 16, 20, 24, 28, and 32 mm day^{-1}) for (a) NoTop, and (b) NoTopSmSST runs. The corresponding 2-month mean SSTs (contours at 1°C intervals) are also plotted.

cific humidity by transporting dry air downward. About 500 km away from the coast, boundary layer moisture recovers to values high enough for convection to become active west of 95°W.

In the NoTop run, humidity does not change much across Central America, except near the surface (Fig. 11b). This dip in boundary-layer humidity is due to precipitation near the east coast (~2 mm day^{-1}; Fig. 9) and weak evaporation supply over land. Without mountains, moisture depletion by precipitation on the Caribbean side of Central America is greatly reduced (Fig. 10), and so is the subsidence on the Pacific side. Both effects act to increase moisture in the lower atmosphere over the Pacific Ocean near Central America in the NoTop compared to the CTL run. The warming and drying induced by orographic subsidence on the

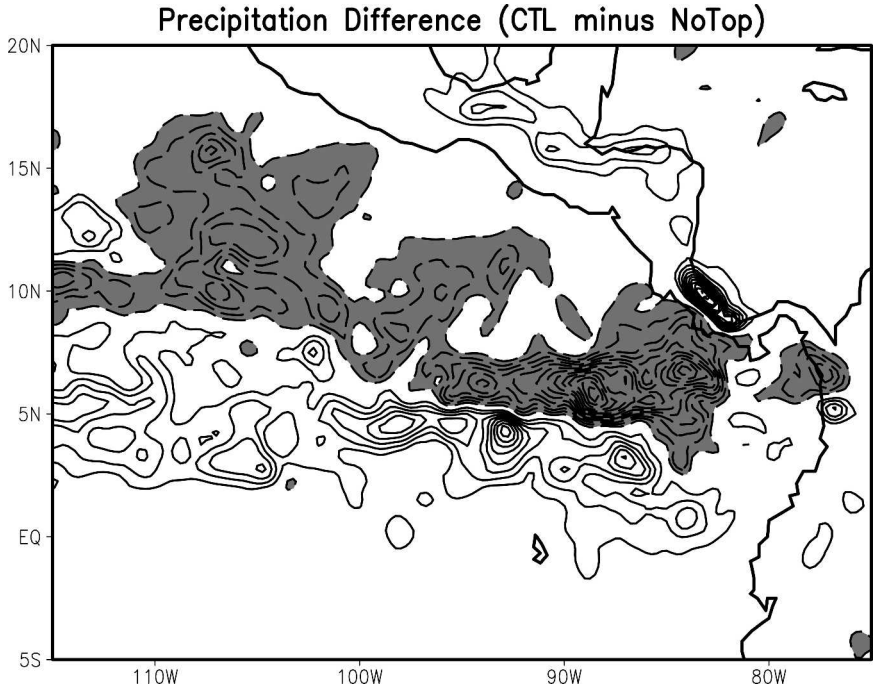

FIG. 10. Difference of precipitation (mm day^{-1}) between the CTL and NoTop runs, averaged for Jan and Feb 2002. Contour interval is 2 mm day^{-1} and values less than –2 mm day^{-1} are shaded.

Pacific reach as far as 400 km offshore, amounting to 2°C and -2 g kg^{-1} in magnitude, respectively (Fig. 11d). The leeward drying effect is further confirmed in column-integrated water vapor difference between the CTL and NoTop runs, with marked negative anomalies off the west coast of Central America (Fig. 12). The orographic effect on moisture is rather modest on the windward side over the Caribbean Sea.

c. SST effects

Surface winds are quite uniform off the west coast of Central America in the NoTop run (Fig. 8), indicating that it may be reasonable to assume that the SST field would also be uniform offshore without the Central American mountain range. Thus, we use an SST field smoothed in the Pacific coastal region (Fig. 4b) to remove both the direct and indirect effects of the Central American mountains on eastern Pacific climate.

The simulated ITCZ in the NoTopSmSST run extends farther to the north compared to that in the CTL and NoTop runs, especially over the Tehuantepec and Papagayo cold patches (Fig. 9b). The smoothed SST field also removes the high SST between the Papagayo and Panama cold patches, weakening the rainband there. Note that while both the direct and indirect effects of mountains are removed in the NoTopSmSST run, convection still does not reach all the way to the Central American coast, with little precipitation in a coastal zone of 100–200 km width (Fig. 9b). This precipitation deficit near the coast seems to be associated with relatively low specific humidity over Central America (Fig. 11c). Low evaporation over the land seems to be insufficient to replace the moisture loss due to precipitation on the east coast of Central America (Fig. 9b), as discussed earlier. It takes about 100–200 km for evaporation over the ocean surface to supply enough moisture for convection.[3] As an additional mechanism for suppressed convection near the coast, surface trade winds accelerate offshore as they blow from the Central America continent to the Pacific

[3] The length for surface evaporation to recharge boundary layer moisture off Central America may be estimated by assuming a simple balance between offshore advection and surface evaporation over the Pacific, $V(\Delta q/\Delta s) = (Q_E/\rho HL)$, where $\Delta q \sim 1.5$ g kg^{-1} is the boundary layer-mean humidity difference between the coast and the offshore ITCZ (Fig. 11c), $V \sim 10$ m s^{-1} is the offshore wind speed, $Q_E \sim 200$ W m^{-2} is the surface latent heat flux, L is the latent heat of vaporization, and $H \sim 1$ km is the boundary layer depth. The offshore distance for humidity to recover is hence $\Delta s = H(\rho LV\Delta q/Q_E) \sim 225$ km, in qualitative agreement with the visual estimate from Fig. 9b. This length for moisture recharge increases with lower coastal humidity, consistent with the southward displacement of the ITCZ in the CTL run.

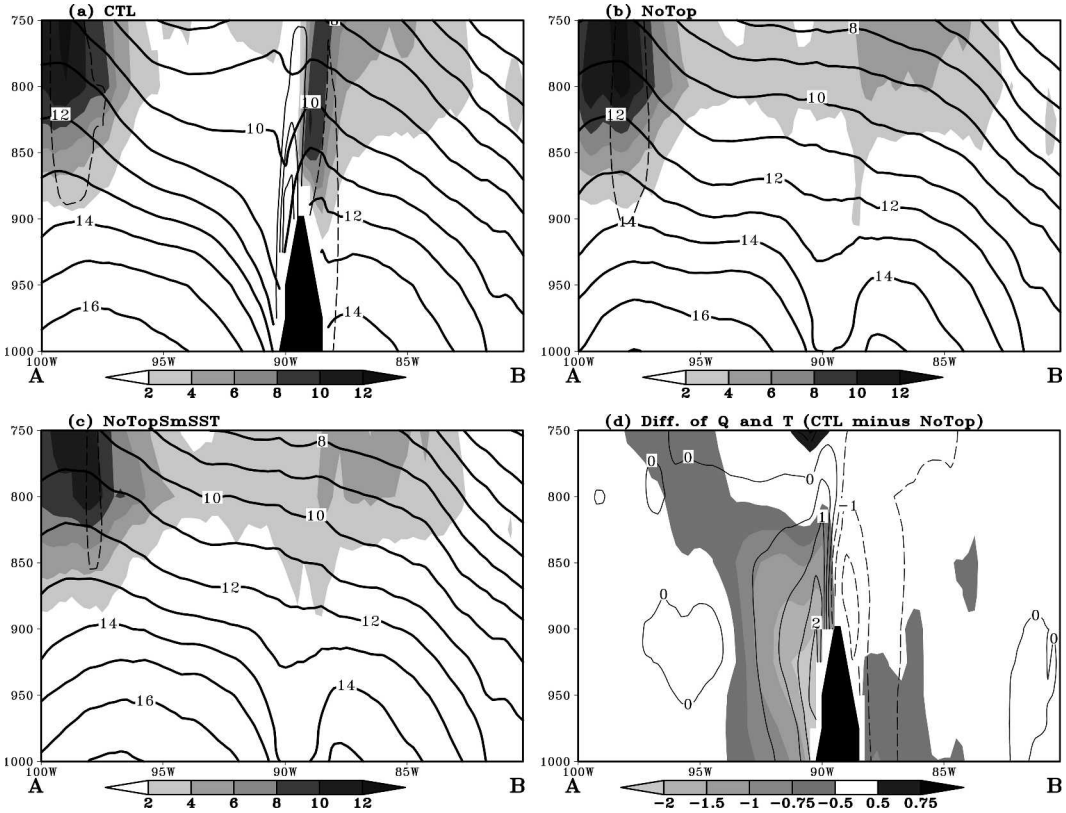

FIG. 11. Vertical cross sections of specific humidity (thick contours at 1 g kg^{-1} intervals), vertical velocity (light contours, interval 0.2 Pa S^{-1} with 0 contour omitted), and cloud liquid water content (shaded at 2×10^{-2} g kg^{-1} intervals) along the line AB in Fig. 4a for (a) CTL, (b) NoTop, and (c) NoTopSmSST runs. The Central American cordillera is shaded black. The differences of temperature (contours at 0.5°C intervals) and specific humidity (shaded, interval levels −2, −1.5, −1.0, −0.75, −0.5, 0.5, and 0.75 g kg^{-1}) between the CTL and NoTop runs are shown in (d).

Ocean because of relatively small surface friction over the ocean in comparison with large surface friction over the land. This coastal divergence zone is rather narrow (not shown) but helps reduce precipitation there.

Figure 13 compares precipitation zonally averaged over the ocean between 110° and 90°W among the CTL, NoTop, and NoTopSmSST runs. Without the direct orographic effect, the latitude of maximum precipitation shifts by about 2° and precipitation increases by 2–4 mm day^{-1} to the north in 8°–18°N. With the indirect orographic/SST effect further removed, the maximum precipitation decrease slightly compared with that in the NoTop run while the precipitation increases both to the north and south in 7°–14°N and in 2°–5°N. In other words, the ITCZ rainband broadens in width, with the region of rain rate above 8 mm day^{-1} extending farther to the north than in the NoTop run.

4. Atlantic-to-Pacific moisture transport

Central American mountains are an important factor in the moisture transport from the Atlantic to the Pacific Ocean. This section investigates the sensitivity of this moisture flux to the representation of orography by comparing results from the CTL and SmTop runs. The moisture transport across the mountain range is approximated by computing the flux perpendicular to a series of line segments approximating the axis of the Central American mountains. The seven linear segments are identified in Table 1 and shown in Fig. 14a, along with the land topography. Our analysis is limited to winter, the season when the Central American gap winds are strongest (e.g., Xie et al. 2005).

Figure 14b shows the January–February 2002 mean column-integrated moisture flux vectors and magnitude from the CTL run. The largest flux occurs across Nicaragua and through the Papagayo gap (segment 5), and geographically the localized maxima in fluxes are closely related to the mountain gaps at Tehuantepec, Papagayo, and Panama (cf. Figs. 3, 14b). The fact that fine structure in the flux field is not seen upstream, to the east of southern Mexico and Central America in the Gulf of Mexico or Caribbean (Fig. 14b) suggests that

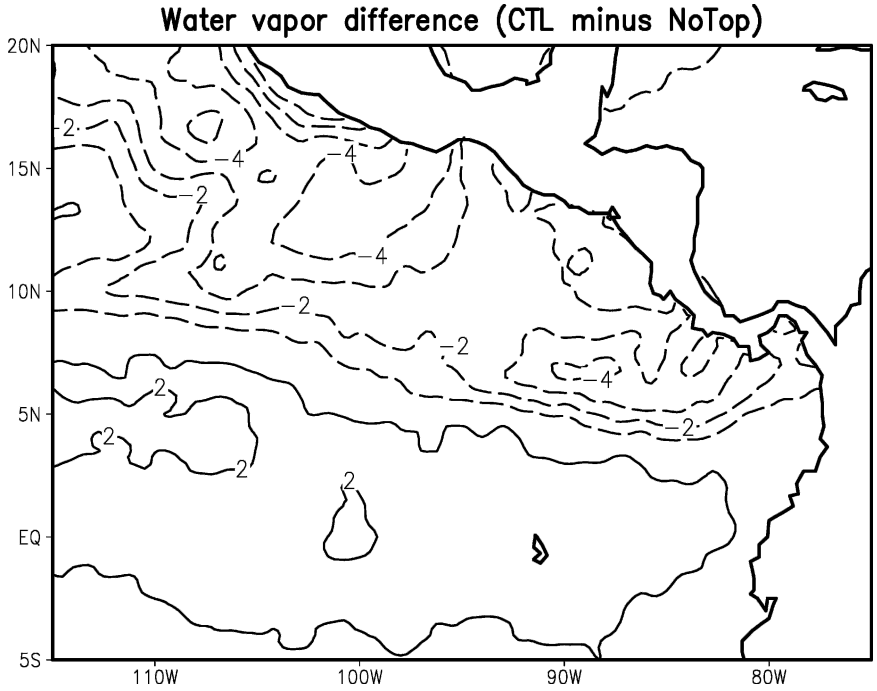

FIG. 12. Difference of column-integrated water vapor (mm) between the CTL and NoTop runs, averaged for Jan and Feb 2002. Contour interval is 1 mm with 0 contour omitted.

the local maxima in fluxes off the Pacific side of Central America are due to local effects. By comparison, the flux in the SmTop run (Fig. 14c) shows less fine structure and a broader maximum in flux spreading westwards from the Nicaragua/Papagayo region, due to the much smoother orography.

The water vapor mixing ratio along the segments, and the wind component normal to the segments (toward the Pacific) are shown as vertical cross sections in Fig. 15 as a function of longitude, with the segment number annotated at the top. The contrast in the orography along the segments (represented as white blocks) between the CTL and SmTop runs is dramatic, and the gaps in the mountain range around 95°W (Tehuantepec), 85°W (Papagayo), and at 79°W (Panama) are more pronounced in the CTL run. As a consequence, the wind speed core through Papagaya is stronger in the CTL run as the flow is squeezed through the narrower gap (Fig. 15).

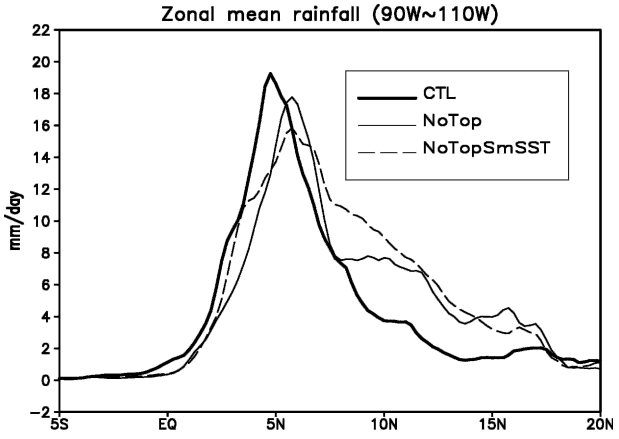

FIG. 13. Precipitation (mm day^{-1}) zonally averaged between 90° and 110°W over the ocean for the CTL (thick solid), NoTop (light solid), and NoTopSmSST (dashed) runs, averaged for Jan and Feb 2002.

TABLE 1. Line integral of flux normal to each segment, for the line segments shown in Fig. 14a. Results show the Jan–Feb 2002 mean from the CTL and SmTop runs.

Segment	Length (km)	Flux (Sv) CTL run	Flux (Sv) SmTop run
1) Sierra Madre Occidental	1553	−0.101	−0.104
2) Tehuantepec gap	550	0.027	0.025
3) Chiapas highlands, South Mexico	232	0.012	0.032
4) Guatemala–Honduras Highlands	465	0.031	0.033
5) Honduras–Nicaragua–Costa Rica/Papagayo gap	767	0.210	0.217
6) Panama	412	0.078	0.046
7) Panama	401	0.066	0.060
Total	4381	0.323	0.309

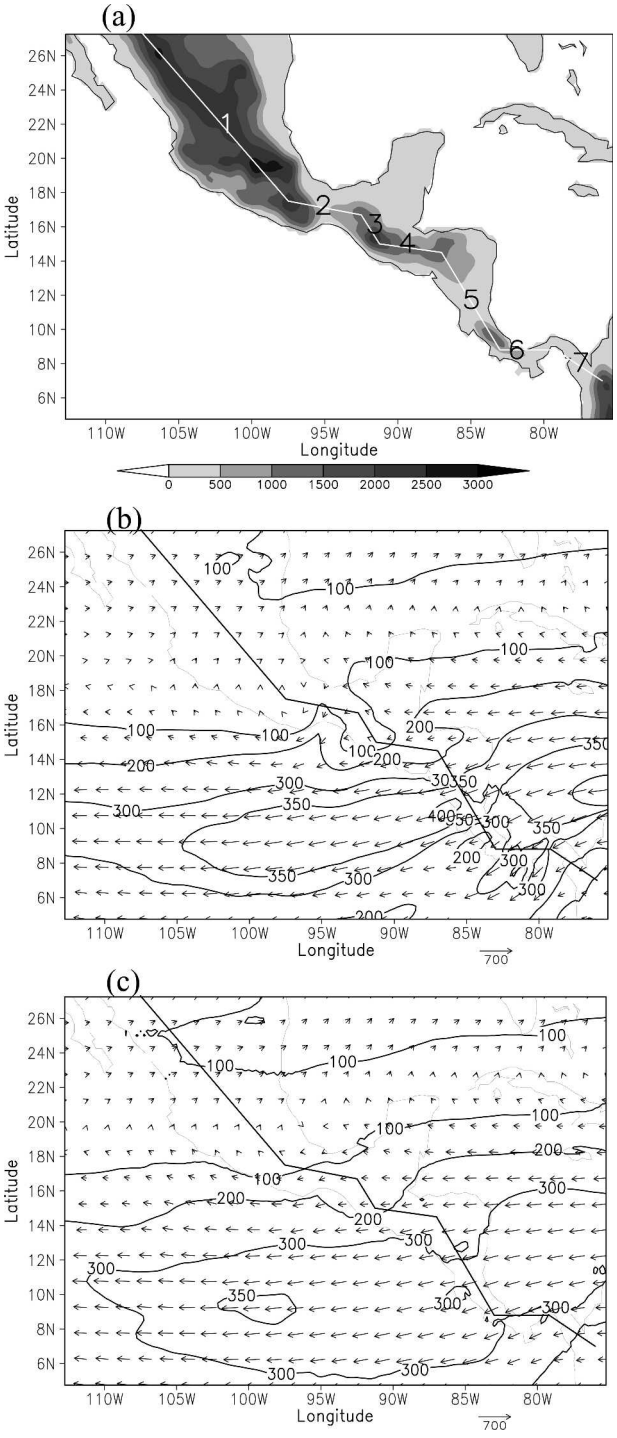

FIG. 14. Column-integrated moisture flux vectors and magnitude in the regional climate model. (a) Topography (shaded, interval 500 m), and location and numbering of line segments (white lines). (b) Jan–Feb 2002 CTL run moisture flux vectors and magnitude in kg m s^{-1} (contour levels 100, 200, 300, 350, and 400 kg m s^{-1}). (c) Same as b but for SmTop run. The vectors are shown every sixth grid point (every 1.5°).

When the component of column-integrated moisture flux normal to the segments (and pointing toward the Pacific), Q, is calculated (Table 1), the largest differences between CTL and SmTop runs occur in segments 3 (south Mexico highlands) and 6 (Panama highlands). In segment 3 the SmTop simulation shows larger Q, due to the absence of the high mountains which would otherwise act to reduce the moisture transport. Along segment 6, Q is reduced in the SmTop run because the smoother Andean mountains weaken the easterly winds to the north in the Caribbean, helping to decrease the moisture fluxes in that area (cf. Figs. 14b,c and note the stronger surface wind component into segment 6 on Fig. 15a). The differences in the segments that include the prominent gaps (2, 5, and 7) are small (Table 1): the stronger flow through the gaps in the CTL run is compensated for by the broader and deeper nature of the flow in the SmTop run (Fig. 15). The overall result is that the total of the flux across Central America mountains is only slightly different between CTL (0.32 Sv, where 1 Sv $\equiv 10^6$ m^3 s^{-1}) and SmTop runs (0.31 Sv).

Not shown here, an analysis of the NCEP–NCAR reanalysis indicates that the moisture transport displays a second peak in July–August when cross–Central American winds intensify (Fig. 1 of Xie et al. 2005) along with a seasonal increase in lower-atmospheric humidity in the region. Thus longer model integrations are necessary to assess the annual-mean moisture transport across Central America and its sensitivity to orography.

5. Summary and discussion

A high-resolution regional climate model is used to study the effects of the Central American mountains on the eastern Pacific ITCZ in boreal winter. The model reproduces the salient features of eastern Pacific climate as compared to TMI and QuikSCAT observations, including three intense wind jets and an ITCZ displaced to the southern edge of the warm pool in the far eastern Pacific. As the strong northeast trades impinge on the Central American mountains, much of the northeast trades is blocked by the mountains. A portion of the trades flows over the mountains and generates subsidence on the leeward side, suppressing atmospheric deep convection over the Pacific Ocean. Experiments with and without Central American cordillera demonstrate that this orographically induced subsidence is the main cause of the southward displacement of the eastern Pacific ITCZ away from the core of the warm pool. Our results also show that cold patches under the gap wind jets, which are themselves an oro-

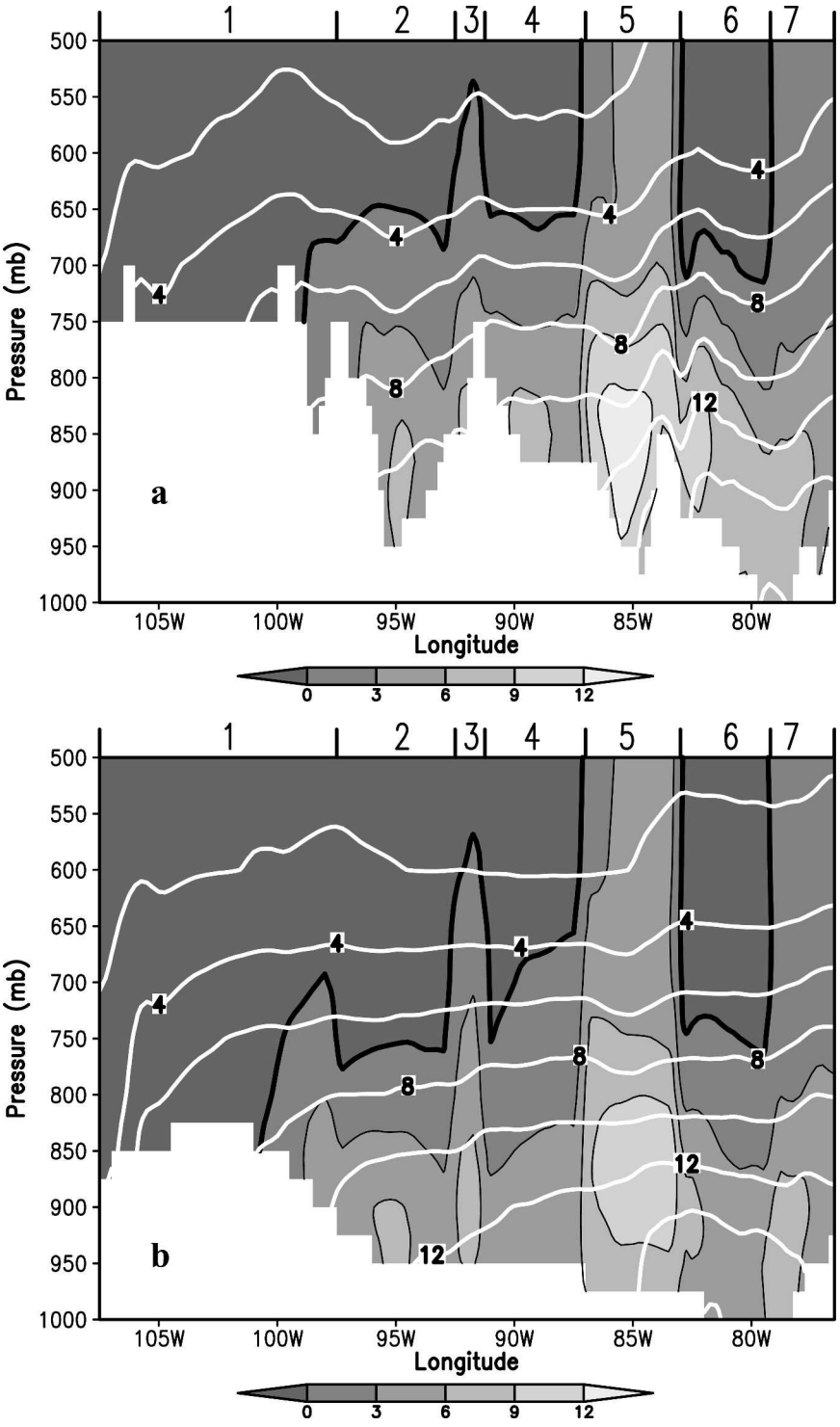

FIG. 15. Vertical cross sections along the line segments shown in Fig. 14, shown as a function of longitude, of velocity normal to the segment, positive denoting toward the Pacific Ocean (shaded, interval 3 m s^{-1}), and water vapor mixing ratio (white contours at 2 g kg^{-1} intervals): (a) CTL run and (b) SmTop run. The zero contour of velocity is emphasized with a thick black line. The location of the segments is shown along the top border.

graphic effect, are an additional mechanism that keeps the ITCZ from moving northward and occupying the warm pool.

While so far we have focused on the winter season, Central American mountains also imprint on the summer climate. Strong curls of gap wind jets imprint on ocean thermocline topography by the Rossby wave mechanism (e.g., McCreary et al. 1989; Umatani and Yamagata 1991). In particular, the cyclonic curls of the Papagayo jet maintain a thermocline dome west of Costa Rica, where the 20°C isotherm is only 30 m deep year-round (Kessler 2002). Xie et al. (2005) show that this thermocline dome maintains a cool spot in the eastern Pacific warm pool and punches a large hole in the ITCZ rainband in summer. Thus, winter gap winds have a delayed effect on eastern Pacific climate in subsequent seasons.

Current GCMs have a typical grid size of 2.8° and do not adequately resolve the narrow mountains of the Americas. In a companion paper, using the same regional model, Xu et al. (2004) study the effects of steep mountains of South America, suggesting that the poor representation of the Andes might be a cause of the systematic bias of many coupled GCMs where the ITCZ persists too long south of the equator (Mechoso et al. 1995). Compared to Central American cordillera, the Andes are much taller in height (>2 km) and block the lower-atmospheric flow, creating favorable conditions for stratus cloud formation by enhancing subsidence offshore. In March–April, the Andes disrupt westward-traveling disturbances that trigger convection, helping terminating the ITCZ south of the equator (Xu et al. 2004). In the 2-month RCM simulations presented here, Central American mountains induce a precipitation dipole offshore (Fig. 10) but has limited effects on winds on and south of the equator based on here. When this RCM is coupled with a general circulation model of the Pacific Ocean, these mountains appear to have significant impacts on the boreal spring ITCZ. Further research is underway with this coupled regional model and its results will be reported elsewhere.

Moisture flux from the Atlantic to the Pacific Ocean is an important component of hydrological cycle, helping set the salinity contrast between the two oceans. The winter wind system is favorable for the Atlantic-to-Pacific moisture transport, with the northeast trades strong on either side of the isthmus. Calculations from the regional climate model showed that around 0.32 Sv of water vapor is transported across the Central American isthmus during January and February 2002. The results of this study suggest that the estimates of this moisture transport is not very sensitivity to the fine structure of the orography (mountain peaks and gaps) because the increased flow in the gaps in detailed topography tends to be compensated for by broader and deeper flow in smoothed topography.

Acknowledgments. We wish to thank Jan Hafner for archiving the TMI and QuikSCAT data from Remote Sensing Systems' Web site and Y. Zhang for archiving the NCEP reanalysis dataset. We are also grateful to anonymous reviewers for their comments, which helped improve the manuscript. This work is supported by NOAA PACS Program (NA17RJ230), NSF (ATM01-04468), NASA (NAG5-10045, JPL1216010), the State Key Program (2004CB418304), and by the Japan Agency for Marine-Earth Science and Technology (JAMSTEC) through its sponsorship of the International Pacific Research Center.

REFERENCES

Broecker, W. S., 1997: The thermohaline circulation, the Achilles heel of our climate system: Will man-made CO_2 upset the current balance? *Science,* **278,** 1582–1588.

Chelton, D. B., M. H. Freilich, and S. N. Esbensen, 2000: Satellite observations of the wind jets off the Pacific coast of Central America. Part II: Regional relationships and dynamical considerations. *Mon. Wea. Rev.,* **128,** 2019–2043.

——, M. G. Schlax, M. H. Freilich, and R. F. Milliff, 2004: Satellite measurements reveal persistent small-scale features in ocean winds. *Science,* **303,** 978–983.

Clarke, A. J., 1988: Inertial wind path and sea surface temperature patterns near the Gulf of Tehuantepec and the Gulf of Papagayo. *J. Geophys. Res.,* **93,** 15 491–15 501.

Detering, H. W., and D. Etling, 1985: Application of the E-ε turbulence model to the atmospheric boundary layer. *Bound.-Layer Meteor.,* **33,** 113–133.

Dickinson, R. E., A. Henderson-Sellers, and P. J. Kennedy, 1993: Biosphere-Atmosphere Transfer Scheme (BATS), Version 1e as coupled to the NCAR Community Climate Model. NCAR Tech. Note NCAR/TN-387+STR, 72 pp.

Edwards, J. M., and A. Slingo, 1996: Studies with a flexible new radiation code. I: Choosing a configuration for a large-scale model. *Quart. J. Roy. Meteor. Soc.,* **122,** 689–719.

Fairall, C. W., E. F. Bradley, D. P. Rogers, J. B. Edson, and G. S. Young, 1996: Bulk parameterization of air-sea fluxes for Tropical Ocean-Global Atmosphere Coupled Ocean Atmosphere Research Experiment. *J. Geophys. Res.,* **110,** 3747–3764.

Gadgil, S., P. V. Joseph, and N. V. Joshi, 1984: Ocean–atmosphere coupling over the monsoon regions. *Nature,* **358,** 394–397.

Giorgi, F., and G. T. Bates, 1989: The climatological skill of a regional model over complex terrain. *Mon. Wea. Rev.,* **117,** 2325–2347.

Graham, N. E., and T. P. Barnett, 1987: Sea surface temperature, surface wind divergence and convection over tropical oceans. *Science,* **238,** 657–659.

Halpern, D., and C.-W. Hung, 2001: Satellite observations of the southeast Pacific intertropical convergence zone during 1993–1998. *J. Geophys. Res.,* **106,** 28 107–28 112.

Hastenrath, S., 1991: *Climate Dynamics of the Tropics.* Kluwer Academic, 488 pp.

Kalnay, E., and Coauthors, 1996: The NCEP/NCAR 40-Year Reanalysis Project. *Bull. Amer. Meteor. Soc.,* **77,** 437–472.

Kessler, W. S., 2002: Mean three-dimensional circulation in the northeast tropical Pacific. *J. Phys. Oceanogr.,* **32,** 2457–2471.

Lau, K.-M., H.-T. Wu, and S. Bony, 1997: The role of large-scale atmospheric circulation in the relationship between tropical convection and sea surface temperature. *J. Climate,* **10,** 381–392.

Legates, D. R., and C. J. Willmott, 1990: Mean seasonal and spatial variability in guage-corrected global precipitation. *Int. J. Climatol.,* **10,** 111–127.

Liu, W. T., X. Xie, P. S. Polito, S.-P. Xie, and H. Hashizume, 2000: Atmospheric manifestation of tropical instability waves observed by QuikSCAT and Tropical Rain Measuring Mission. *Geophys. Res. Lett.,* **27,** 2545–2548.

McCreary, J. P., H. S. Lee, and D. B. Enfield, 1989: Response of the coastal ocean to strong offshore winds: With application to circulations in the Gulf of Tehuantepec and Papagayo. *J. Mar. Res.,* **47,** 81–109.

Mechoso, C. R., and Coauthors, 1995: The seasonal cycle over the tropical Pacific in coupled ocean–atmosphere general circulation models. *Mon. Wea. Rev.,* **123,** 2825–2838.

Mitchell, T. P., and J. M. Wallace, 1992: The annual cycle in equatorial convection and sea surface temperature. *J. Climate,* **5,** 1140–1156.

Mozer, J. B., and J. A. Zehnder, 1996: Lee vorticity production by large-scale tropical mountain range. Part I: Eastern North Pacific tropical cyclogenesis. *J. Atmos. Sci.,* **53,** 521–538.

Nordeng, T. E., 1995: Extended versions of the convective parameterisation scheme at ECMWF and their impact upon the mean climate and transient activity of the model in the Tropics. ECMWF Research Department Tech. Memo. 206, 41 pp.

Pierrehumbert, R. T., and B. Wyman, 1985: Upstream effects of mesoscale mountains. *J. Atmos. Sci.,* **42,** 977–1003.

Reynolds, R. W., and T. M. Smith, 1994: Improved global sea surface temperature analyses using optimum interpolation. *J. Climate,* **7,** 929–948.

——, N. A. Rayner, T. M. Smith, D. C. Stokes, and W. Wang, 2002: An improved in situ and satellite SST analysis for climate. *J. Climate,* **15,** 1609–1625.

Serra, Y. L., and M. J. McPhaden, 2003: Multiple time- and space-scale comparisons of ATLAS buoy rain gauge measurements with TRMM satellite precipitation measurements. *J. Appl. Meteor.,* **42,** 1045–1059.

Small, R. J., S.-P. Xie, and Y. Wang, 2003: Numerical simulation of atmospheric response to Pacific tropical instability waves. *J. Climate,* **16,** 3722–3737.

Steenburgh, W. J., D. M. Schultz, and B. A. Colle, 1998: The structure and evolution of gap outflow over the Gulf of Tehuantepec, Mexico. *Mon. Wea. Rev.,* **126,** 2673–2691.

Sun, Z., and L. Rikus, 1999: Improved application of exponential sum fitting transmissions to inhomogeneous atmosphere. *J. Geophys. Res.,* **102,** 6291–6303.

Tiedtke, M., 1989: A comprehensive mass flux scheme for cumulus parameterization in large-scale models. *Mon. Wea. Rev.,* **117,** 1779–1800.

Umatani, S., and T. Yamagata, 1991: Response of the eastern tropical Pacific to meridional migration of the ITCZ: The generation of the Costa Rica Dome. *J. Phys. Oceanogr.,* **21,** 346–363.

Waliser, D. E., and N. E. Graham, 1993: Convective cloud systems and warm-pool sea surface temperatures: Coupled interaction and self-regulation. *J. Geophys. Res.,* **98,** 12 881–12 893.

Wang, C., S.-P. Xie, and J. A. Carton, 2004: A global survey of ocean-atmosphere and climate variability. *Earth Climate: The Ocean-Atmosphere Interaction*, *Geophys. Monogr.,* No. 147, Amer. Geophys. Union, 1–19.

Wang, Y., 2001: An explicit simulation of tropical cyclone with a triply nested movable mesh primitive equation model: TCM3. Part I: Model description and control experiment. *Mon. Wea. Rev.,* **129,** 1370–1394.

——, O. L. Sen, and B. Wang, 2003: A highly resolved regional climate model (IPRC–RegCM) and its simulation of the 1998 severe precipitation event over China. Part I: Model description and verification of simulation. *J. Climate,* **16,** 1721–1738.

——, S.-P. Xie, H. Xu, and B. Wang, 2004: Regional model simulations of boundary layer clouds over the Southeast Pacific off South America. Part I: Control experiment. *Mon. Wea. Rev.,* **132,** 274–296.

Wentz, F. J., C. Gentemann, D. Smith, and D. Chelton, 2000: Satellite measurements of sea surface temperature through clouds. *Science,* **288,** 847–850.

Woodruff, S. D., R. J. Slutz, R. L. Jenne, and P. M. Steurer, 1987: A comprehensive ocean–atmosphere data set. *Bull. Amer. Meteor. Soc.,* **68,** 1239–1250.

Xie, P., and P. A. Arkin, 1996: Analyses of global monthly precipitation using gauge observations, satellite estimates, and numerical model predictions. *J. Climate,* **9,** 840–858.

Xie, S.-P., 2004a: Satellite observations of cool ocean-atmosphere interaction. *Bull. Amer. Meteor. Soc.,* **85,** 195–208.

——, 2004b: The shape of continents, air-sea interaction, and the rising branch of the Hadley circulation. *The Hadley Circulation: Past, Present and Future,* H. F. Diaz and R. S. Bradley, Eds., Kluwer Academic, 121–152.

——, H. Xu, W. S. Kessler, and M. Nonaka, 2005: Air-sea interaction over the eastern Pacific warm pool: Gap winds, thermocline dome, and atmospheric convection. *J. Climate,* **18,** 5–25.

Xu, H., Y. Wang, and S.-P. Xie, 2004: Effects of the Andes on eastern Pacific climate: A regional atmospheric model study. *J. Climate,* **17,** 589–602.

Zhang, C., 2001: Double ITCZs. *J. Geophys. Res.,* **106,** 11 785–11 792.